Microstructure and mechanical properties of a laser powder bed fused Al-Fe alloy

Yann Le Bouar, Louise Toualbi, Frederic Fossard, Jean-Sébastien Mérot, Pauline Stricot, Simon Fritz, Agnes Bachelier-Locq, Nicolas Horezan, Quentin Barres, Maria Tsoutsouva, et al.

Microstructure and mechanical properties of a laser powder bed fused Al-Fe alloy.

Y. Le Bouar[2], L. Toualbi[1], F. Fossard[2], J.-S. Mérot[2]; P. Stricot[1,2], S. Fritz[1,2], A. Bachelier-Locq[1]; N. Horezan[1], Q. Barres[1], M. Tsoutsouva, M. Fèvre, C. Davoine[1], M. Thomas[1]

[1] Université Paris-Saclay, ONERA, DMAS, Châtillon, France
[2] Université Paris-Saclay, ONERA, CNRS, LEM, Châtillon, France

Abstract
The Laser Powder Bed Fusion process features very short interactions between the powder and the laser, resulting in very high solidification and cooling rates. During thermal cycling in L-PBF processing, phase precipitation and thermal strain hardening occur concomitantly, thus leading to high dislocation density correlated with anchoring to precipitates. It is therefore important to understand and control precipitation kinetics with respect to the thermal strain hardening phenomena generated by the thermal cycles of the L-PBF process. This issue concerns in particular structural hardening materials, such as nickel-based superalloys and aluminium alloys. The aim of this study is to understand the thermal, metallurgical and mechanical phenomena generated during the manufacture of a model aluminum alloy by L-PFB, in order to evaluate the impact of thermal strain hardening on the precipitation of the strengthening phases. A fine microstructural characterization using scanning electron microscopy and transmission electron microscopy shows a strong interaction between dislocation density and precipitation.

Introduction
In recent years, the advent of additive manufacturing techniques has allowed a considerable gain in terms of manufacturing costs, especially for parts with complex geometries. The L-PBF process studied here allows the elaboration, by a succession of lasering passes on a powder bed, of metal parts, which can present geometries difficult to achieve with conventional manufacturing techniques. However, the microstructure of the as-built parts depends not only on the parameters of the FA process used, but also on the thermal specificities of this process. In the case of the L-PBF process, which is characterized by particularly short laser-material interaction times, the as-manufactured microstructures are generally far from equilibrium, and characterized by a high dislocation density [1]. Up to now, industrialists have been trying to obtain microstructural and mechanical properties for the parts obtained by FA that are comparable to those obtained by conventional manufacturing and shaping processes. It is therefore necessary to find a suitable heat treatment to apply to the post manufacturing parts [2-8].
However, an increasing number of studies are tending to propose grades specially designed to meet the specificities of additive manufacturing processes [9-11]. For example, in the case of the families of metal alloys with structural hardening, the nanometric precipitation of hardening phases takes place concomitantly with a pinning of dislocations resulting from the thermal process on these same precipitates [12-14]. The resulting hardening, linked to both thermal hardening and alloy chemistry, can be of great benefit, especially if it avoids the need for a post manufacturing heat treatment.
In the framework of this study, the case of aluminium alloys with structural hardening is considered. The aim is to study a model alloy, the binary alloy Al-Fe, and of being interested in the interactions between the dislocations resulting from the thermal processing and the nanoprecipitates present from the first stages of the solidification, and which are found in the as-built microstructures.

Experimental procedure
The material of this study is a binary aluminum alloy with a nominal composition of Al-4Fe (wt%). The rapid solidification in the L-PBF process enables the formation of very fine precipitates which are known to improve both strength and ductility of these alloys [14-15]. Therefore, this model system enables the study of the correlated apparition of high dislocation densities resulting from the thermal work hardening of the L-PBF process and the hardening nanoprecipitates specific to this family of alloys. This characteristic is particularly interesting for the definition of a process/material couple allowing to avoid the implementation of a post-production thermal treatment. It has also been found that by limiting the number of alloying elements, a good compromise between mechanical and thermal properties can be achieved, hence the interest in using binary or ternary alloys in the case of aluminum parts made by Additive Manufacturing [9].
The studied samples were manufactured by L-PBF using different parameters. Without being able to give the details of the parameters used, the main modifications concerned the plateau heating temperature, the vector gap and the feed rate, with the aim of inducing a modification of the thermal phenomena undergone by the material.

The study of the microstructure organization requires the use of complementary characterization techniques, at different scales of interest. Thus, optical microscopy is used to visualize the trace of the melt pool. Scanning electron microscopy characterizations allow imaging the largest precipitates. Electron BackScatter Diffraction analysis gives access to the morphology of the grains and their crystallographic orientation. Finally, the fine characterization carried out by transmission electron microscopy allows highlighting the solidification substructures, as well as the finest precipitates, which appeared at the first stages of solidification.
The evaluation of thermal hardening is a particularly delicate subject, which remains open [16]. We propose to couple fine and localized measurements of Vickers micro-hardness to a local analysis of intragranular disorientations, obtained from EBSD maps. In perspectives of the work presented in this paper, we propose to use transmission electron microscopy to visualize the dislocations, and in particular, their interactions with precipitates, in order to propose hypotheses about the hardening mechanisms involved.
The evolution of this non-equilibrium microstructure will also be studied following the implementation of different post manufacturing thermal treatments. The aim is not only to study the stability of the thermal hardening resulting from the L-PBF process, but also the precipitation and growth kinetics of the phases present in the as-built microstructure. Thus, a matrix of thermal treatments has been proposed and carried out.

Microstructure characterization
The optical micrographs made in the building direction give a good visualization of the melt pools and of the different layers (Figure 1-left). The transverse direction features discontinuous beads, , due to the three-dimensional morphology of the beads and to a partial melting of the previous layer during the passage of the laser of the current layer (Figure 1-right). It also reveals the 67° rotation of the scan directions between the successive layers, used to prevent the development of single-crystalline-like texture [17].

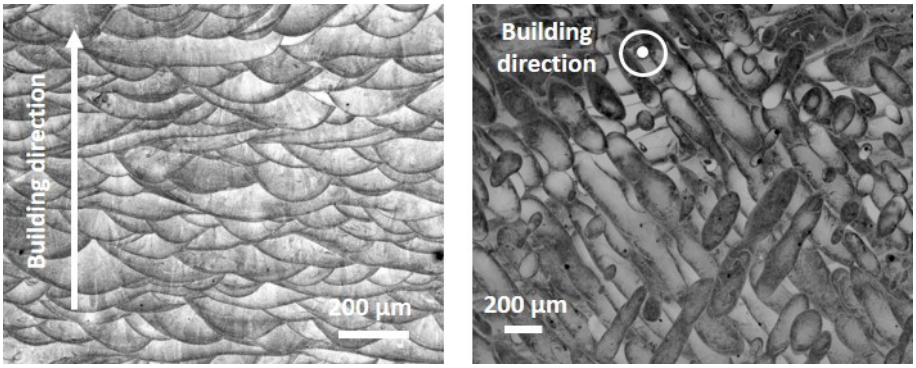

Figure 1. Optical micrographs of Al-4Fe L-PBF samples in parallel i.e. building (left) and transverse (right) directions.

Scanning electron microscopy characterization also shows an epitaxial growth of columnar grains through the melt pools (**Error! Reference source not found.**-left). EBSD characterization permits a better visualization of the grain shape. We may note the presence of finer grains at the border of the melt pool. We observe that the epitaxial growth of columnar grains can pass through several melt pools (Figure 2-right). These EBSD measurements also give access to an average estimation of the grain size. Given their elongated morphology, this average value is only indicative. Thus, we estimate that in their smallest dimension, the elongated grains have an average width of 50 µm.

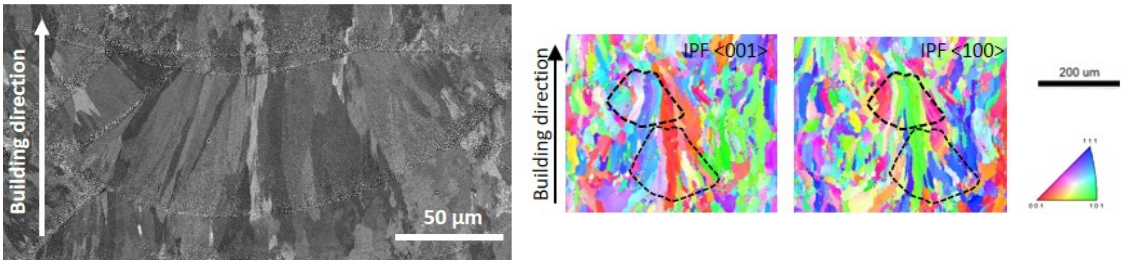

Figure 2. SEM image in BSE mode of one melt pool (left) and EBSD IPF maps of several melt pools of Al-4Fe L-PBF samples in building direction.

Figure 3 reveals that the border of the melt pools is decorated by a micrometric precipitation, which appears in white on the images. These precipitates probably play the role of nucleant, inducing the presence of the finer grains at the border of the melt pool as described above.

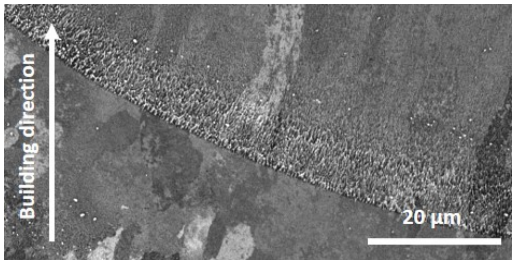

Figure 3. SEM image in BSE mode of micrometric precipitation at the border of a melt pool of an Al-4Fe L-PBF sample in building direction.

With further analysis by scanning electron microscopy, we detect the presence of three different zones, in terms of size of microstructure (Figure 4). The first one, which corresponds to a remelted zone, is a zone with a coarse microstructure, located at the bottom of the melt pool, where the cooling rate is the lowest. We can note the presence of micrometric precipitates visible in this coarse zone. The second one, which corresponds to a heat-affected zone, is a zone where the temperature increases but not to the melting point, inducing slight evolutions of the microstructure, in this case a slight coarsening of the cell-like structure. The third one, which was melted only once, is a zone with a very fine microcellular structure. Many authors classically point out the presence of these different zones in L-PBF as-built Al-Fe samples [11,14,18]. Some prefer to differentiate only two of them, the remelted zone and the fine zone, and then mention a gradual refinement of the cell-like structure. Other authors identify a third intermediate zone, thermally affected, which presents distinct microstructural characteristics [19-20].

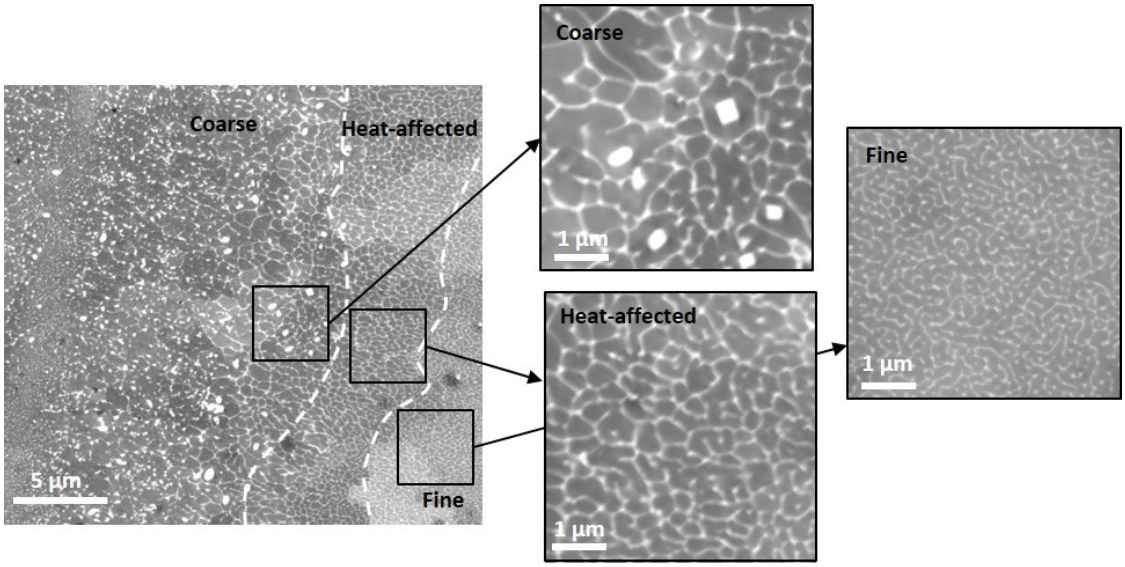

Figure 4. SEM images in BSE mode of the three different zones of an Al-4Fe L-PBF sample.

The fine characterization of the microstructure by transmission electron microscopy reveals a solidification in cell-like structure. EDS chemical analyses in HAADF (High Angle Annular Dark Field) mode show that the iron segregates at the border of the sub-cells (Figure 5). Furthermore, we can see that the thermal cycling induced by the L-PBF process results in different subcell sizes.

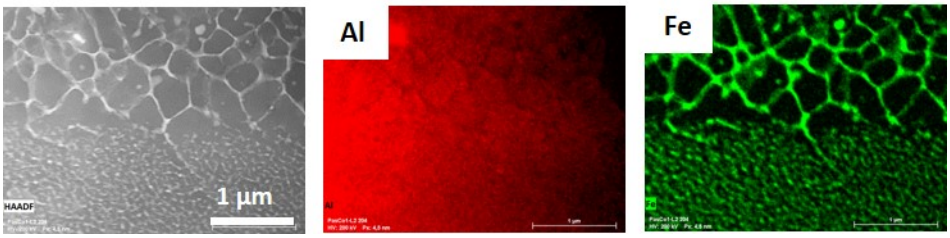

Figure 5. STEM images in HAADF mode (left) showing EDS Al and Fe chemical maps of the cell-like structure in an Al-4Fe L-PBF sample.

We can see the presence of precipitates of different shapes and sizes whose distribution in the microstructure is not homogeneous. In the bottom of the melt pool, we have already seen that we have some coarse precipitates, visible in scanning electron microscopy (Figure 3). Within the heat-affected zones, we find some fine precipitates, of a few hundred nanometers (Figure 6). At least, in the so-called fine microstructure zone, which seemed to be without precipitates, we can detect at high magnification, precipitates of a few nanometers (Figure 6). It has to be noted that these characteristics are found on all the samples, independently of the manufacturing parameters used.
The nanoprecipitates that have been highlighted in the ultrafine microstructure zones are those that are likely to interact with the dislocations resulting from the thermal cycling of the L-PBF process to induce an interesting hardening. Figure 6 shows two types of precipitates, whose interactions with dislocations depend on their size.

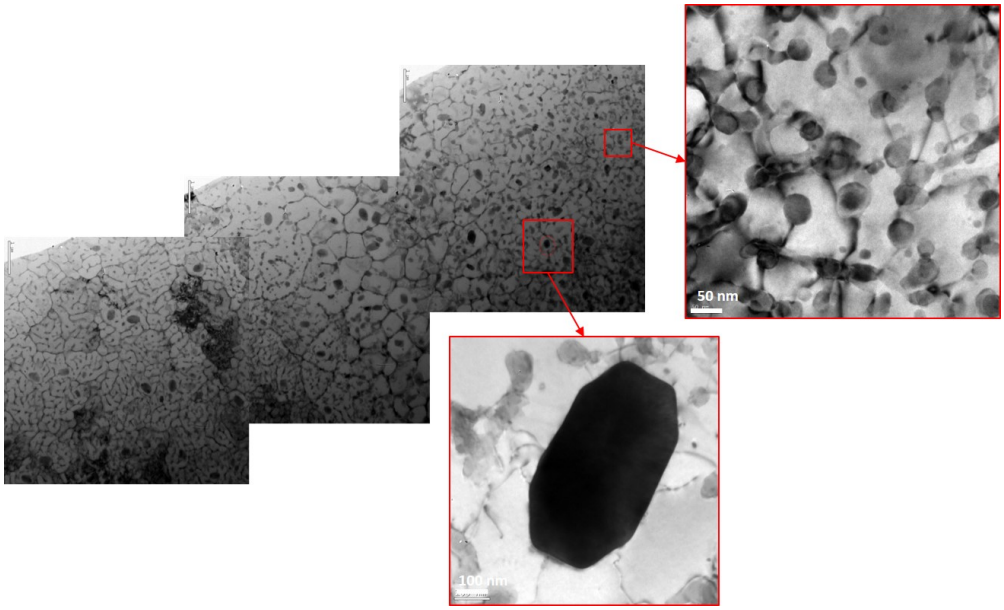

Figure 6. TEM images in Bright Field mode showing the interaction between dislocations and precipitates in an Al-4Fe L-PBF sample.

Concerning the different L-PBF parameters used to manufacture the samples of this work, the main result is that, despite the presence of columnar grains highlighted by the EBSD maps, none of our samples show any cracks along the High Angle Grain Boundaries. This can be explained by the absence of segregation at the grain boundaries at the end of solidification.

Thermal treatment post-fabrication
Different post manufacturing heat treatments are being investigated. The objective of this work is to evaluate the stability of the microstructure, in terms of grain size, precipitate coarsening and thermal hardening. The treatment temperatures are between 250°C and 600°C, for durations ranging from 2h up to 20h. For the time being, only a few first samples could be characterized. It can be seen that a treatment at 600°C for 6h induces a significant coarsening of the precipitates (Figure 7-upper left). On the counterpart, the heat treatments carried out at 250°C show a remarkable stability of the microstructure, and this for all the durations, in particular 20h of holding at temperature (Figure 7-upper right and bottom). As pointed out by Qi *et al.* in an Al-2.5Fe alloy, even after 1000h of thermal exposure at 300°C, a considerable number of nanosized precipitates remain. No significant grain growth occurs, which can be explained by the pinning effect of these fine precipitates on the grain boundary, preventing their migration [21].

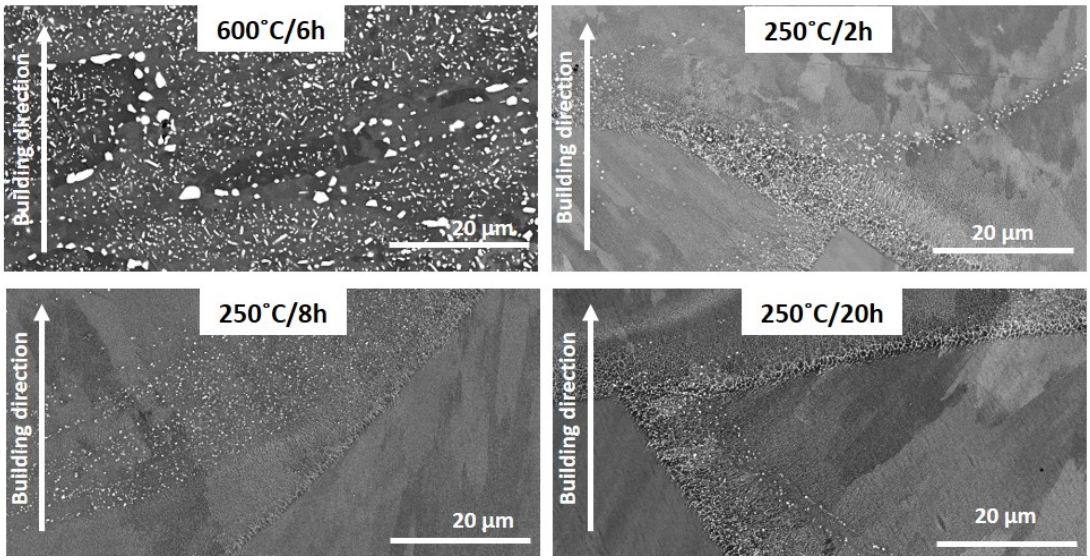

Figure 7. SEM images in BSE mode of micrometric precipitation at the border of a melt pool of four heat-treated Al-4Fe L-PBF samples in building direction.

Estimation of the thermal hardening

Vickers micro-hardness measurement is one of the techniques used to evaluate the level of hardening of the as-built samples. The microstructural analysis having shown a strong heterogeneity, it appears important to carry out hardness measurements in similar zones of the microstructure. Thus, measurements were made in the center of the melting baths and other measurements at the border. The tests are performed with an applied load equal to 100 g which leads to a footprint of several tens of micrometers, as shown in the Figure 8. The area impacted by the indentation is therefore of the same order of magnitude as the average grain width (about 50 µm,) but smaller than the size of the melt pool.

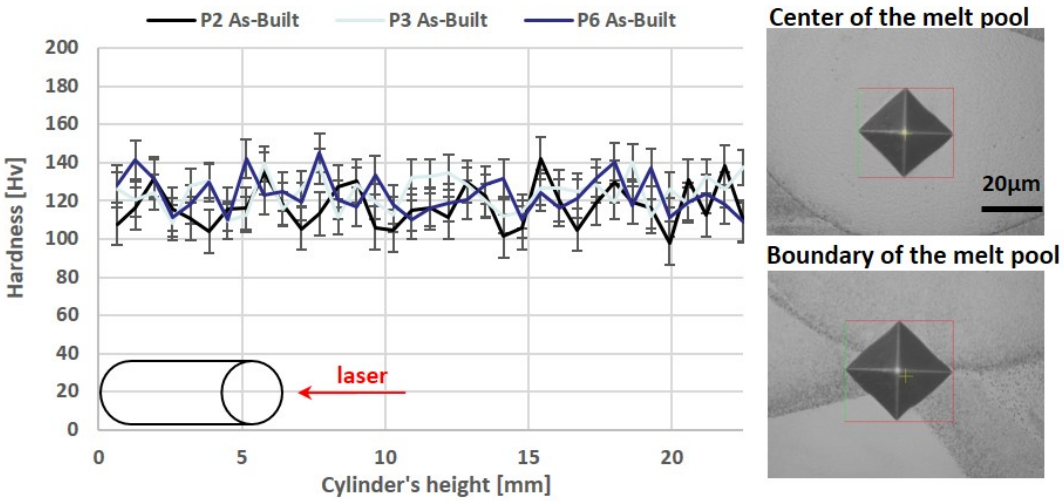

Figure 8. Vickers micro-hardness measurements on as-built Al-4Fe L-PBF samples obtained with three different manufacturing parameters.

In average, the Vickers micro-hardness measurements at the center of the melt are 20 points higher than those obtained at the border. Indeed, as shown in the **Error! Reference source not found.**, the border of the melt pool is the area with the highest density of micrometric precipitates. By contrast, in the center of the melt, we find nanometric precipitates that seem to participate more effectively in the hardening process, particularly by pinning dislocations. The effect of the presence of iron in solid solution can also be considered to explain these differences in hardness, but the solubility of iron in the crystalline lattice of aluminum is so limited that this hypothesis seems not very robust. Even taking into account the microstructure variations due to the specific organization induced by the L-PBF process, the hardness values show a relatively large standard deviation. On the other hand, we note that considering this standard deviation, the variation in hardness between the three manufacturing

conditions is low, all samples featuring a Vickers micro-hardness value around 120. This shows the good robustness of this alloy with respect to the manufacturing conditions.
The second technique used to estimate the thermal hardening induced by the L-PBF process is the analysis of intragranular misorientations from the EBSD maps [22]. Thus, maps processed in Kernel Average Misorientation mode were obtained with a step size of 300 nm to estimate the residual thermal hardening of the as-built samples. Figure 9 shows the maps obtained for three different processing conditions: the KAM values calculated are globally low, meaning that the residual thermal hardening is not as high as we thought, probably because of the pre-heating of the plate. Futhermore, it seems that the measurement noise is too large to obtain a reliable quantitative analysis [23]. New analyses, with a refined step size, could allow a better estimation of the thermal hardening on these as-built samples [24]. These EBSD characterizations will also be coupled with TEM and ECCI observations, which will allow a better quantification [25-27]. Here again, the variation in residual thermal hardening between the three manufacturing conditions is very small, proving the robustness of the alloy at the intragranular scale.

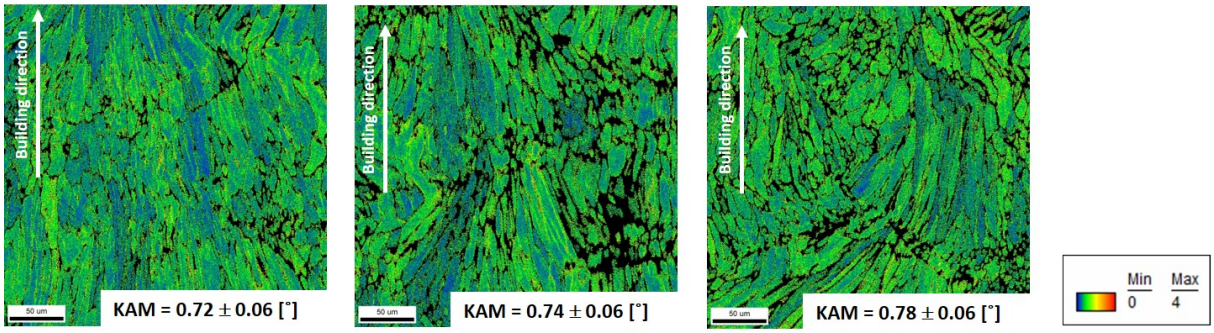

Figure 9. EBSD KAM maps on as-built Al-4Fe L-PBF samples obtained with three different manufacturing parameters.

Conclusion

This preliminary study shows the interest of a complete control of the relationships between thermal, metallurgical and mechanical phenomena. Indeed, the gain in terms of mechanical strength that can be obtained by defining an aluminum alloy grade dedicated to Additive Manufacturing is significant. It allows benefiting from the double advantage of an anchoring of dislocations resulting from the thermal cycling of L-PBF process on nanoprecipitates themselves hardening. The manufacturing without cracking phenomena, the possibility to use simplified post processing thermal treatments and the stability of the microstructure with respect to the processing parameters are all elements of major interest for the industrials.
The next step in this study will be to compare samples with higher levels of work hardening, in order to validate the interest of using the KAM method of analysis from the EBSD maps. One of the ambitions of this work is also to study the interactions between dislocations and nanoprecipitates present in the early stages of solidification. We will be interested in comparing the dislocations resulting from a thermal phenomenon via the comparison of specimens presenting different levels of thermal hardening due to a modification of the manufacturing parameters L-PBF, and the dislocations of strain hardening resulting from a mechanical solicitation, in this case via the application of compressive stresses on the studied samples.

Reference

[1] W.J. Sames et al., *The metallurgy and processing science of metal additive manufacturing*, (2016) International Materials Reviews
[2] Z. Zhao, *Microstructure and mechanical properties of laser additive repaired Ti17 titanium alloy*, Trans. Nonferrous Met. Soc. China 27 (2017) 2613-2621.
[3] X. Lin et al., *Microstructure and mechanical properties of laser forming repaired 17-4PH stainless steel*, Materials Science and Engineering A 553 (2012) 80– 88.
[4] M.R. Rokni et al., *The effects of heat treatment on 7075 Al cold spray deposits*, Surface & Coatings Technology 310 (2017) 278-285.
[5] X. Fang et al., *Microstructure evolution of wire-arc additively manufactured 2319 aluminum alloy with interlayer hammering*, Materials Science & Engineering A 800 (2021) 140168.
[6] C. Guevenoux et al., *Influence of interlayer dwell time on the microstructure of Inconel 718 Laser Cladded components*, Optics and Laser Technology 128 (2020) 106218.

[7] N. E. Uzan, R. Shneck, O. Yeheskel, N. Frage, *High-temperature mechanical properties of AlSi10Mg specimens fabricated by additive manufacturing using selective laser melting technologies (AMSLM)*, Additive Manufacturing 24 (2018) 257–263
[8] N. Takata, M. Liu, H. Kodaira, A. Suzuki, M. Kobashi, *Anomalous strengthening by supersaturated solid solutions of selectively laser melted Al–Si-based alloys*, Additive Manufacturing 33 (2020) 101152.
[9] B. Chehab, S. Unnikrishnan, *A new aluminium alloy for PBF-LB*, Metal Additive Manufacturing, Vol. 8 No. 1.
[10] M. Buttard, B. Chehab, R. Shahani, F. Robaut, G. Renou, C. Tassin, E. Rauch, P. Donnadieu, A. Deschamps, J.J. Blandin, G. Martin, *Multi-scale microstuctural investigation of a new Al-Mn-Ni-Cu-Zr aluminium alloy processed by laser powder bed fusion*, Materialia 18 (2021) 101160.
[11] W. Wang, N. Takata, A. Suzuki, M. Kobashi, M. Kato, *High-temperature strength sustained by nano-sized eutectic structure of Al–Fe alloy manufactured by laser powder bed fusion*, Materials Science & Engineering A 838 (2022) 142782.
[12] T. Vilaro et al., *Microstructural and mechanical approaches of the selective laser melting process applied to a nickel-base superalloy*, Materials Science & Engineering A 534 (2012) 446-451.
[13] D. Zhang et al., *Effect of standard heat treatment on the microstructure and mechanical properties of selective laser melting manufactured Inconel 718 superalloy*, Materials Science & Engineering A 644 (2015) 32-40.
[14] W. Wang, N. Takata, A. Suzuki, M. Kobashi, M. Kato, *Formation of multiple intermetallic phases in a hypereutectic Al–Fe binary alloy additively manufactured by laser powder bed fusion*, Intermetallics 125 (2020) 106892.
[15] X. Qi, N. Tanaka, A. Suzuki, M. Kobashi, M. Kato, *Managing both high strength and thermal conductivity of a laser powder bed fused Al–2.5Fe binary alloy: Effect of annealing on microstructure*, Materials Science & Engineering A 805 (2021) 140591.
[16] M. Kamaya, *Assessment of local deformation using EBSD: Quantification of accuracy of measurement and definition of local gradient*, Ultramicroscopy 111 (2011) 1189–1199.
[17] S.-H. Sun, K. Hagihara, T. Nakano, *Effect of scanning strategy on texture formation in Ni-25 at.%Mo alloys fabricated by selective laser melting*, Materials and Design 140 (2018) 307–316.
[18] X. Qi, N. Takata, A. Suzuki, M. Kobashi, M. Kato, *Laser powder bed fusion of a near-eutectic Al–Fe binary alloy: Processing and microstructure*, Additive Manufacturing 35 (2020) 101308.
[19] S.B. Sun, L.J. Zheng, J.H. Liu, H. Zhang, *Selective Laser Melting of an Al-Fe-V-Si Alloy: Microstructural Evolution and Thermal Stability*, Journal of Materials Science & Technology 33 (2017) 389-396.
[20] R.A. Michi, A. Plotkowski, A. Shyam, R.R. Dehoff, S. S. Babu, *Towards high-temperature applications of aluminium alloys enabled by additive manufacturing*, International Materials Reviews (2022) 67:3, 298-345
[21] X. Qi, N. Takata, A. Suzuki, M. Kobashi, M. Kato, *Change in microstructural characteristics of laser powder bed fused Al–Fe binary alloy at elevated temperature*, Journal of Materials Science & Technology 97 (2022) 38–53.
[22] J. Jiang, T.B. Britton, A.J. Wilkinson, *Measurement of geometrically necessary dislocation density with high resolution electron backscatter diffraction: Effects of detector binning and step size*, Ultramicroscopy 125 (2013) 1–9.
[23] C. Moussa, M. Bernacki, R. Besnard, N. Bozzolo, *About quantitative EBSD analysis of deformation and recovery substructures in pure Tantalum*, Materials Science and Engineering 89 (2015) 012038.
[24] S.I. Wright, D.P. Field, M.M. Nowell, *Post processing effects on GND calculations from EBSD-based orientation measurements*, Materials Science and Engineering 89 (2015) 012049.
[25] C. Moussa, M. Bernacki, R. Besnard, N. Bozzolo, *Statistical analysis of dislocations and islocation boundaries from EBSD data*, Ultramicroscopy 179 (2017) 63–72.
[26] Z. Wang, J. Gu, D. An, Y. Liu, M. Song, *Characterization of the microstructure and deformation substructure evolution in a hierarchal high-entropy alloy by correlative EBSD and ECCI*, Intermetallics 121 (2020) 106788.
[27] J. Zhang, B. Wang, H. Wang, *Geometrically necessary dislocations distribution in face-centred cubic alloy with varied grain size*, Materials Characterization 162 (2020) 110205.